IVYSPRING INTERNATIONAL PUBLISHER

Theranostics

2017; 7(9): 2377-2391. doi: 10.7150/thno.19408

Research Paper

An [^{18}F]-Positron-Emitting, Fluorescent, Cerebrospinal Fluid Probe for Imaging Damage to the Brain and Spine

Harikrishna Kommidi[1], Hua Guo[1], Nandi Chen[1, 2], Dohyun Kim[3], Bin He[3], Amy P. Wu[4], Omer Aras[5]✉, and Richard Ting[1]✉

1. Department of Radiology, Molecular Imaging Innovations Institute (MI3), Weill Cornell Medical College, New York, NY 10065, USA;
2. State Key Laboratory of Chemo/Biosensing and Chemometrics, College of Chemistry and Chemical Engineering, Key Laboratory for Bio-Nanotechnology and Molecular Engineering of Hunan Province, Hunan University, Changsha 410082, China;
3. Department of Radiology, Weill Cornell Medical College, New York, NY 10065, USA;
4. Department of Otolaryngology – Head & Neck Surgery, Northwell Health, Hofstra Northwell School of Medicine. New York, NY, 10075, USA;
5. Department of Radiology, Memorial Sloan Kettering Cancer Center, New York, NY, 10065, USA.

✉ Corresponding authors: Richard Ting, Molecular Imaging Innovations Institute (MI3), Department of Radiology, Weill Cornell Medical College, 413 East 69th Street. New York, NY 10065, USA, E-mail: rct2001@med.cornell.edu TEL: 6469626195 FAX: 6469620577 or Omer Aras, Department of Radiology, Memorial Sloan Kettering Cancer Center, New York, NY, 10065, E-mail: araso@mskcc.org. TEL: 6468884690 FAX: 6468884915

Received: 2017.01.30; Accepted: 2017.03.22; Published: 2017.06.15

Abstract

Fluorescein is modified to bear ^{18}F so that it can act as both a positron emitter, and a fluorophore, allowing detection by positron emission tomography (PET), scintillation, and fluorescent imaging (FL). [^{18}F]-**2** is injected into the intrathecal space of rats and used to observe the cerebrospinal fluid (CSF) that bathes the brain and spine. Injury in three different applications is visualized with [^{18}F]-**2**: 1) detection of a 0.7 mm paranasal-sinus CSF leak (CSFL); 2) detection of 0.5 mm puncture damage to the thoracic spine (acute spinal cord injury); and 3) detection of intracerebral hemorrhage/edema because of traumatic brain injury. In all models, the location of injury is visualized with [^{18}F]-**2** at high resolution. [^{18}F]-**2** PET imaging may be a superior alternative to current clinical contrast myelography and ^{131}I, ^{111}In or ^{99m}Tc radionuclide cisternography. Like fluorescein, [^{18}F]-**2** may also have other uses in diagnostic or fluorescence guided medicine.

Key words: Positron emission tomography, imaging, optical imaging, radionuclide cisternography, myelography.

Introduction

Damage to the central nervous system (CNS) can significantly reduce a patient's quality of life, especially if not promptly addressed. Dural tears in the CNS lead to neural inflammation, loss of sensory function, intracranial hypotension, meningitis, brain herniation, paralysis and coma [1]. Unfortunately, CNS injuries can be difficult to identify, especially in patients who are unconscious, unresponsive, or have spontaneous, non-acute injury, where injury is not obvious by computed tomography (CT) or magnetic resonance (MR) imaging. Spontaneous cerebrospinal fluid leaks (CSFL) are misdiagnosed at a high rate (94%), with a long average diagnostic delay of up to 13 months [2].

A popular method for indicating CNS damage involves introducing a contrast agent into the CNS via the cerebrospinal fluid (CSF) [3]. In a healthy patient, the CSF is compartmentalized to the CNS in a well-defined, anatomical volume [4]. Damage to the thin layer of tissue encapsulating the CNS (arachnoid and dura mater) results in the leakage of the CSF into spaces that would not normally contain CSF. Because CSF leakage closely accompanies CNS damage, one should be able to infer and precisely identify a site of CNS damage by imaging aberrant CSF flow. In addition to imaging trauma, one could use a CSF

imaging agent to observe device placement or blockage in lumbar and ventriculoperitoneal shunts [5-7].

Surgeons often choose to diagnose and repair a dural tear in a fluorescence-guided surgery that is rapid (vs. non-fluorescent CSFL repair). This is accomplished through the injection of intrathecal fluorescein (IF) [3, 8, 9]. A dural tear is diagnosed through the detection of fluorescein in the nasal cavity (potentially in-office), using an inexpensive, ultraviolet light emitting diode [3, 8, 9]. Fluorescein is contained at the site of CSF fluid, where its fluorescent properties can be used to diagnose and monitor a leak, or guide and confirm surgical repair [9]. Unfortunately, in paranasal sinus CSF tears, IF has drawbacks including a high false negative rate (26.2%) [3], and in the case of a non-obvious CSF leak, additional follow-up imaging, including single photon emission computed tomography (SPECT)/ cisternography, CT, or MR [10, 11] is required to precisely identify the site of CNS damage for targeted repair [12-14].

Fluorescein (D & C yellow no. 7, Fluorescite, Ak-fluor, or Ful-glo, Scheme 1) is of interest to medicinal chemists as it is one of the first, and one of few current, highly fluorescent agents that is approved for clinical use (indocyanine green, and porfimer sodium are two others). Were a [^{18}F]-PET/fluorescent multimodality imaging probe to be approved for clinical use, it follows that this probe would share structural similarities with fluorescein, because of already-demonstrated safety and utility *in vivo*. Initially approved for imaging vessels in the eye, fluorescein's use has expanded to many applications in medicine [15, 16], including CSFL repair [3, 8, 9].

We report the synthesis of a fluorescein derivative, [^{18}F]-**2**, that is labeled with ^{18}F [17-20], a positron emission tomography (PET) isotope (Scheme 1). This multimodality imaging agent would be the first ^{18}F-PET agent for diagnosing CSFL. It has properties that make it superior to current stand-alone fluorescent agents (fluorescein). PET has an advantage over SPECT agents due to the higher spatial resolution and sensitivity of PET imaging systems. The ability to image CSFL in deep tissue suggests that [^{18}F]-**2** can be used as a general tool for diagnosing trauma to the brain and spine.

Results

Chemical synthesis

We choose to incorporate an alkylammoniomethyltrifluoroborate trap ($AMBF_3$) [21] onto fluorescein. This technology for acid catalyzed isotopic ^{18}F-^{19}F exchange-radiolabeling is compatible with direct fluorophore radiolabeling [19, 22-24]. [^{19}F]-**2**, the $AMBF_3$ bearing derivative of fluorescein is described in Scheme 1 and is synthesized in a 2-step synthesis. Fluorescein isothiocyanate, a fluorescein derivative is conjugated with 4-azido butylamine through $CuSO_4$ and sodium ascorbate catalyzed Huisgen 1,3-dipolar cycloaddition. **2** is isolated with an overall yield 34 % (280 mg). The fluorescent properties of [^{19}F]-**2** are like fluorescein (pH 7.5, 1x PBS, Table 1 (Supporting figure S1, S2)). At physiological pH (1x PBS, pH 7.5), the following spectral properties are observed; an extinction coefficient of 90 000 M^{-1} cm^{-1} (Figure 1a $\varepsilon_{max\ nm}$ = 493), an excitation maximum λ= 495 nm, an emission maximum λ= 511 nm (Figure 1a, stokes shift = 16 nm). [^{19}F]-**2** has a quantum yield of φ = 0.28, which is 73% of fluorescein. The $AMBF_3$ and its linker do not alter fluorescein's fluorescent properties. During copper catalyzed 1,3,-dipolar cycloaddition, thiourea hydrolysis was observed. The conversion of the thiourea moiety on [^{19}F]-**2** into urea can be driven by strong base (sodium hydroxide) treatment or heating at high temperatures in mild base like ammonium hydroxide. The urea derivative of **2** is not the focus of this manuscript, and was not tested. It is assumed that the urea derivative of **2** would give similar *in vivo* data. When [^{19}F]-**2** is cyclized in the absence of a base catalyst, no urea [^{19}F]-**2** formation was observed (experimental section). All imaging studies were performed with the pure thiourea, **2**.

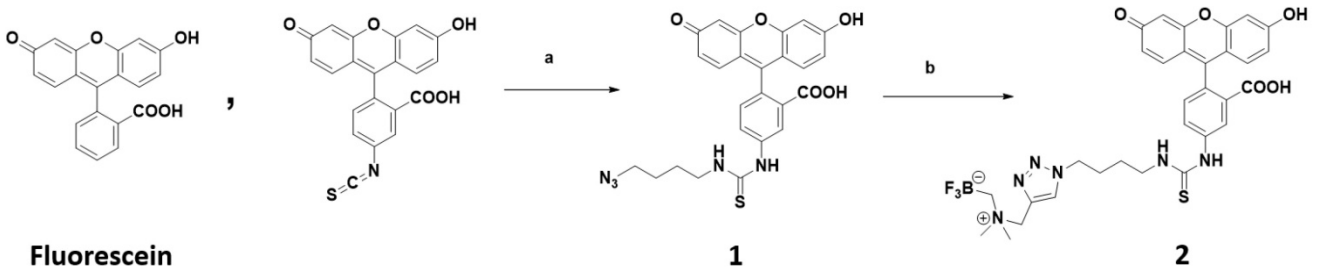

Scheme 1. Fluorescein and scheme for a fluorescein-bearing alkylammoniomethyltrifluoroborate 2. Reagent and conditions: (a) 1.2 eq. 4-Azidobutan-1-amine, DMF, RT, 12h; (b) N,N-Dimethyl-N-Propargyl-N-Methyltrifluoroborate, 1.0M $CuSO_4$ 5 H_2O, 1.0 M Sodium ascorbate, DMF, 50°C, 6 hours. Radiolabeling: **2** is added to a water-DMSO mixture of pyridazine–HCl 1.25 M, pH 2.5 and [^{18}F]- fluoride ion. It is heated at 50-100°C for 10-30 min.

Table 1. Spectral properties of [$^{18/19}$F]-**2** were tested along-side fluorescein (Aldrich F2456) in pH 7.4 water (1x PBS buffer), and in sodium hydroxide (solid) dissolved in absolute ethanol.

	pH / buffer	λ_{max} (nm) (5-6 µM solution)	ε ($cm^{-1}M^{-1}$) (5-6 µM solution)	Excitation (nm)	Emission (nm)	Stokes Shift (nm)	Quantum yield (φ)
Fluorescein	1x PBS (pH 7.4)	490	89 090	494	508	14	0.38
[^{19}F]-**2**	1x PBS (pH 7.4)	493	89 636	495	511	16	0.28
Fluorescein	0.1 M NaOH/EtOH	489	81 666	501	520	19	0.95
[^{19}F]-**2**	0.1 M NaOH/EtOH	489	88 909	500	522	22	0.61

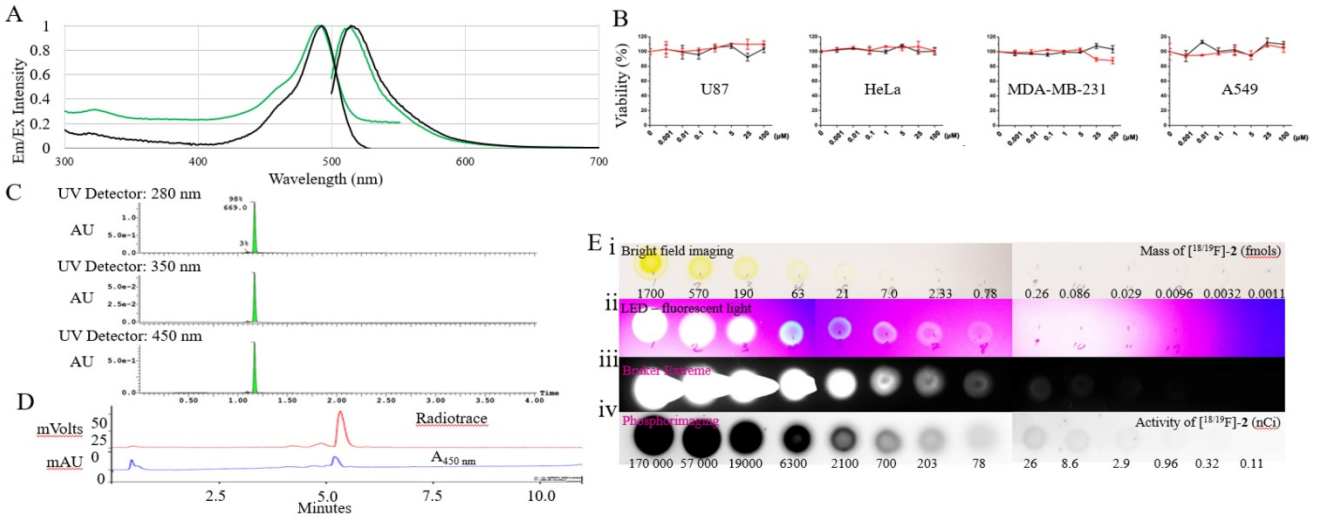

Figure 1. Spectral and radioactive properties of [$^{18/19}$F]-**2.** (A) Excitation and emission spectra of 5-6 µM solutions of fluorescein (black) and [$^{18/19}$F]-**2** (green) in 1x PBS, pH 7.4 measured on a Cary Eclipse spectrophotometer, with 5 nm slit widths, and excitation at 490 nm. (B) *In vitro* cell viability tests performed with compound **2** (red line) and fluorescein (control) 24 hour on U87, Hela, MDA-MB-231, and A549 immortal cell lines using a CellTiter 96® AQueous One Solution Cell Proliferation Assay (MTS, G3582, Promega). Toxicity is not observed. (C) UV-Vis (280, 350, and 450 nm) UPLC-MS of **2** on a waters Acuity UPLC and a Phenomenex Luna Kinetex 1.7 µm EVO C18 50 x 2.1 mm column (00B-4726-AN), with a 1.5 min, a10-90% H_2O:ACN (0.05% TFA) elution gradient indicating a pure synthesis of **2**. (D) Reverse phase HPLC of radiolabeled [^{18}F]-**2** on a Varian HPLC, using an Waters SunfireTM C18 3.5 µm 4.6 x 50 mm column (186002551), a10-90% H_2O:ACN (0.05% TFA) elution gradient and a flow rate of 2 mL/min. (E) 10 µL 3x dilution series of [$^{18/19}$F]-**2** beginning at 70 µM (1.7 pmols) and 170 µCi of [$^{18/19}$F]-**2** (first spot). A 10 µl volume was plated onto glass-backed TLC plate model. Imaging was performed using (i) bright-field; (ii) a UV-sight hand-held 4.5 volt LED black-light (fluorescence); (iii) a Bruker Xtreme optical imaging device (fluorescence: 1 sec acquisition using excitation and emission filters set at λex= 450 nm and λem= 535 nm); (iv) and a phosphorimager.

In vitro toxicity assays

To show that [^{19}F]-**2** is non-toxic *in vitro*, **2** was co-incubated with different immortal cell lines Figure 1b. The effect of **2** on these cells were assayed using CellTiter 96® AQueous One Solution Cell Proliferation Assay (MTS, G3582, Promega). Like fluorescein, toxicity was not observed even when 100 µM aliquots of **2** were incubated with cells for 24 hours.

Radiochemistry

The radiolabeling of [^{19}F]-**2** is performed in ~60 min. 31.3 mCi of [^{19}F]-**2** (400 mCi/µmol) is isolated from 116 mCi of fluoride ion (Figure 1e). Compound **2**, bears an $AMBF_3$ moiety whose synthesis is described by Perrin [17], and radiochemical observations are similar [17]. Isotope exchange is pH dependent, insensitive to water, and proceeds faster at higher temperatures. The trifluoroborate is stable for periods greater than 7 days (half-life of $t_{1/2}$ of defluoridation) in ^{19}F-fluoride NMR defluoridation tests performed *in vitro* [25, 26], where **2** is incubated with PBS, or FBS (Supporting Figure S3, S4, S5). Mono or difluoroborate intermediates are not isolated or observed. Note that *in vitro* stability does not guarantee absolute stability *in vivo*, however, researchers studying trifluoroborate PET imaging see minimal *in vivo* instability [17, 27]. Boronic acid (5 ± 5%) is observed upon lyophilization of **2**, or extended heating. Boronic acids can be separated from **2** by HPLC (0.5 to 1 min shift a10-90 % 20 min, HPLC). The mixture can be converted back into the trifluoroborate, **2**, with the stoichiometric addition of fluoride. Boronic acid bearing **2**, does not bear ^{18}F and cannot be observed by PET.

Detection limits of fluorescence and scintigraphy

A 10 µL 3x dilution series of **2** containing 170 µM (1.7 pmols) and 170 µCi of [$^{18/19}$F]-**2** (first spot) were plated onto glass-backed TLC plates (Silica Gel 60, EMD Millipore, F254, Figure 1e). Three imaging

devices were used to approximate the limits of detection of [$^{18/19}$F]-**2**; an inexpensive UV-sight hand-held 4.5 volt LED black-light (fluorescence); a Bruker Xtreme optical imaging device (fluorescence: 1 sec acquisition time using excitation and emission filters set at λ_{ex}= 450 nm and λ_{em}= 535 nm); and a Phosphorimager (Cyclon, PerkinElmer) (15 min exposure). Fluorescence could be detected in quantities above 0.86 fmols (0.57 picograms) by LED black-light under continuous illumination, 0.0096 fmols (0.0064 picograms) on the Bruker Xtreme in a 20 second capture, and above 1 nCi by phosphorimaging. Note that these detection limits are approximate, and likely overestimate sensitivity *in vivo*, as light scattering and non-specific absorption in the presence of blood and tissue are expected to interfere with *in vivo* fluorescence detection. We note that a Ludlum model 44-9 GM pancake detector is more sensitive at detecting trace quantities of [^{18}F]-**2** vs. phosphorimaging.

Intrathecal introduction of 2

Sprague Dawley (7-9 weeks, 220-300 g, n = 40) rats were used for this project. Rats of both sexes were used, but sex-specific cohorts were not designated. Rats (n = 14) were intrathecally injected with [^{19}F]-**2**. All agents were dissolved in 1x PBS pH 7.65, centrifuged in an Eppendorf 5424R centrifuge at 14000 rpm for 1 min, and passed through a 0.22 µm syringe filter before being introduced intrathecally. Volumes of up to 600 µL were introduced into rats via an implanted intrathecal catheter using an infusion pump set to deliver 10 µL/min. Infusion could be performed on the PET/CT, during the PET phase of a PET/CT scan (Supporting Video S1). The catheter can be optionally removed.

In survival studies (n = 10, [^{19}F]-**2**; and n = 2, PBS controls), acute toxicity associated with [^{19}F]-**2** was not observed. Compound [^{19}F]-**2**'s solubility in 1x PBS is 2 mM. At the highest injected volume, 600 µL of saturated (2 mM) [^{19}F]-**2** was delivered intrathecally into rats. Control intrathecal injections were performed using 1x PBS alone. All (100%, n=12) rats that receive an intrathecal injection of [^{19}F]-**2** survive after recovery from anesthesia. Morbidity was not observed in rats where [^{19}F]-**2** had been infused. An expected symptom of morbidity due to [^{19}F]-**2** is long term hind limb impairment, as tissue in the lumbar spine (the infusion site) receives the largest concentration of [^{19}F]-**2**. This was not observed. The following traits (which were not observed) were monitored for daily in rats infused with [^{19}F]-**2**, beginning at 2-weeks post-surgery: limp effecting the hind limbs, inability to rear symmetrically (the rat could squarely bear their body weight on their hind limbs), and unequal bilateral range of motion in hind limbs. Trembling was sometimes observed following immediate recovery from anesthesia. We suspect trembling is due to transient hypothermia or is anesthesia linked because it would cease within 4 hours and not recur. Rats injected with [^{19}F]-**2** fully recover from surgery and survive for up to 1 month (n=10, end-point of survival experiments). Weight-gain following surgery and intrathecal injection of [^{19}F]-**2** do not deviate from intrathecal PBS-only controls.

Trauma models

To demonstrate a general utility in diagnosing injury to the brain and spine, [^{18}F]-**2** was tested in three trauma models.

CNS trauma model #1: Iatrogenic anterior skull base CSFL

For imaging a paranasal-sinus cerebrospinal fluid leak (CSFL), rats were first injected intrathecally with 20 to 100 µCi of [^{18}F]-**2** (Figure 2a, Supporting Figure S7). All images were acquired using Siemens Inveon PET/SPECT/CT scanner. Dynamic video of intrathecal injection is included in Supporting Video S1 and S2. After a 10 min CT scan and a 30 min PET scan, rats were sacrificed by CO_2 overdose followed by bilateral thoracotomy to ensure euthanasia. A 3 inch, 22-gauge needle (0.7176 mm), was then inserted into the left nostril of the deceased rat. The bore of this needle could be optionally filled with Ficoll-Paque anti-coagulant (GE). In a swift single motion that runs parallel to the superior slope of the skull, the needle was driven through the nasal sinus, olfactory bulb, and neocortex to rest on the rear parietal bone of the rat. This procedure is highly reproducible, as needle motion is both limited and guided by the nasal and premaxilla structures. A PET/CT scan was acquired, with the lodged needle, to show left-sided, proper puncture of the wall between the sinus and the olfactory bulb (cribriform plate, ethmoid bone) Figure 2b.

In rats bearing intrathecal [^{18}F]-**2**, asymmetric drip of [^{18}F]-**2** into the left paranasal sinus (indicating a left-side CSF tear draining into the left sinus) is clearly visible (Figure 2b). The CSF tear became more apparent when the needle is removed (Figure 2c, Supporting Figure S8, Supporting Video S3). CSFL is clearly left-sided, and the PET signal would allow a surgeon to target this site for repair. In addition to asymmetric CSF pooling in the rat's left nasal sinus, CSF flow-through to the esophagus is observed by PET, and rhinorrhea collected from the nostrils and mouth (using gauze placed under the rat's head) is both fluorescent and observable by PET.

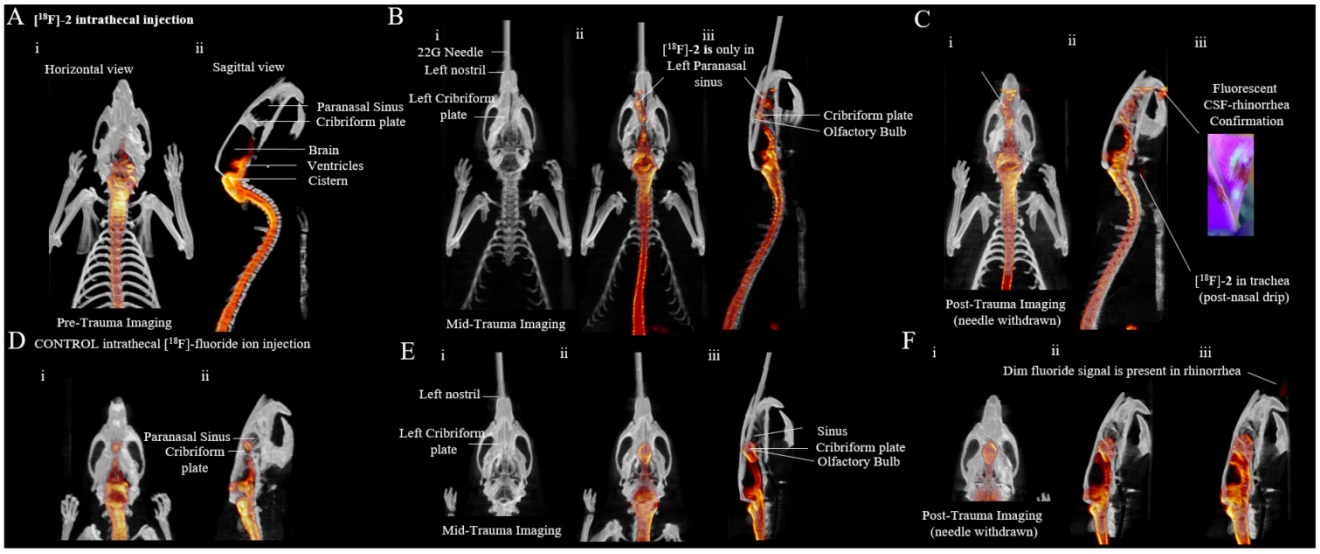

Figure 2. [18/19F]-**2** is used to identify the site of an iatrogenic anterior skull base CSF leak. (A) Pre-trauma imaging of intrathecally injected [18/19F]-**2** (50 µCi). (i) PET data (red) are all maximum intensity projections overlaid on 1 cm to 2.5 mm CT sections (white) (ii) [18F]-PET/CT sagittal views. All PET data are shown as maximum intensity projections. All CT are 2.5 mm sections. [18/19F]-**2** is clearly visible in the spine, ventricles and cisterns. Note that PET signal is not observed in the paranasal sinus that is separated from the CSF by the cribriform plate. (B) Mid-trauma imaging of intrathecally injected [18/19F]-**2**. A 22G needle is passed through the left nostril to pierce the cribriform plate to induce CSF leakage from the olfactory bulb into the paranasal sinus (i) CT imaging showing the 22G needle in the left sinus. (ii) Horizontal PET/CT showing asymmetrical [18/19F]-**2** distribution that is clearly in the left paranasal sinus cavity. (iii) Sagittal PET/CT showing needle placement and PET signal in the paranasal sinus. (C) Post-trauma imaging acquired after the removal of the needle. (i) horizontal PET/CT, and (ii) sagittal PET/CT. (iii) CSF as a result of trauma can be collected in rhinorrhea and imaged by both PET and fluorescence. **(D-F) CONTROL imaging using [18F]-fluoride ion (200 µCi).** (D) Pre-trauma imaging of a rat injected intrathecally with [18F]-fluoride ion (i) horizontal and (ii) sagittal imaging. (E) CONTROL Mid-trauma imaging of intrathecally injected [18F]-fluoride ion. (i) CT showing that a needle is passed through the left nostril to pierce the cribriform plate. CSF leak into the paranasal sinus is not indicated with [18F]-fluoride ion in (ii) horizontal or (iii) sagittal PET/CT. Asymmetric tracer distribution into the left paranasal sinus is not observed (the site of leakage cannot be localized and it is not clear that the trauma is on the left) in (F) CONTROL post-trauma in (i) horizontal and (ii) sagittal PET/CT imaging. (iii) extreme windowing of the PET signal shows minor quantities of [18F]-fluoride ion in rhinorrhea. [18F]-fluoride ion is not fluorescent. Scale bar = outer diameter of 22G needle in B and E is 0.7176 ± 0.0064 mm. 5 rats were used in this study. (Additional replicates in supporting information S12, S13)

As a control, [18F]-**2** was substituted with a much higher radioactive dose (200 µCi) of [18F]-fluoride ion, which was also introduced intrathecally (Figure 2d). [18F]-fluoride ion is inferior to [18F]-**2**. Asymmetric CSFL into the left nostril is not observed (Figure 2e, i.e., it is not clear if CSFL is in the right or left paranasal sinus), and only a minor quantity of activity was detected in rhinorrhea (Figure 2f). Accumulation of [18F]-fluoride ion at the cribriform plate is observed. This nonspecific accumulation may complicate CSFL detection. In Figure 2D-F, an asymmetric lesion to the left sinus is not obvious in CT or PET/CT. [18F]-fluoride ion cannot be used to localize a CSF leak in this model. Note that we attempt control imaging with 100 µCi of intrathecal [99mTc]-DTPA (Supporting figure S14, Supporting Video S8) but fail to obtain adequate SPECT/CT images on our Inveon micro SPECT/CT scanner.

CNS trauma model #2: Acute spinal cord injury

To image puncture damage to the thoracic spinal cord (acute spinal cord injury), a catheter was placed into the intrathecal space of a rat. The fascia and muscle layers around thoracic vertebrae T7-T9 were dissected and a T8 laminectomy was performed. This rat was then euthanized by CO_2 overdose followed by bilateral thoracotomy to ensure euthanasia. On the deceased rat, a 25-gauge needle (0.5144 mm) was used to pierce the dura between thoracic vertebrae T7 and T8. The rat was placed in the Inveon PET/CT scanner for a 10 min CT acquisition followed by a 40 min PET acquisition. During the 40 min PET acquisition, 100 µCi of [18F]-**2** was infused through the catheter. Reconstructions of the acquired PET/CT data show a sharp defect between thoracic vertebrae T7 and T8 in the PET and PET/CT images indicating the site of puncture (Figure 3). This puncture is only observable by [18F]-**2** PET (Supporting Video S5) and is not indicated by vertebrae displacement in stand-alone CT (Figure 3, Supporting Video S4).

CNS trauma model #3: Traumatic brain injury

The CSF encompasses the entire brain, so a head injury resulting from an external force that perturbs CSF flow should be detectable with [18F]-**2**. A liquid nitrogen cryoprobe can be used to generate traumatic brain injury (TBI) with accompanying intracerebral hemorrhage [28]. We recently report the use of Raslan's TBI murine model [29] in imaging hemorrhage using RBCs [30]. To image traumatic brain injury using [18F]-**2**, a catheter was placed into the intrathecal space of a rat [31]. Using a liquid nitrogen cooled, 2 mm diameter, aluminum tipped cryoprobe [30], asymmetric injury is generated over the right neocortex of the lumbar-catheter-bearing rat. The right exposed skull over the neocortex was

contacted for 2 min using 400 g of mass. Following cryolesion, 100 μCi of [^{18}F]-**2** was infused into cryolesion bearing rats that were placed on their back, with their head and TBI down, through an intrathecal lumbar injection (This imaging will not work if rats are injected upright (on their feet), as CSF flow is driven by gravity, and accumulation in the cisterns and ventricles will obscure signal at the TBI). Following infusion, 1 hour-post cryolesion, the rat was euthanized, the brain was excised and placed on a petri dish. Bright light photography was used to capture non-symmetric, right-brain hematoma that result from cryolesion (Figure 4a). The excised brain was placed in the Inveon PET/CT scanner, and confirmative, [^{18}F]-PET/CT imaging was used to corroborate asymmetric hematoma that is visible by bright field imaging (Figure 4b, Supporting Video S6). Asymmetric accumulation of [^{18}F]-**2** is observed at the site of cryolesion. Intrathecal [^{19}F]-**2** injection and fluorescence histology was performed on a section containing the neocortex and olfactory bulb of a healthy-control rat showing that there is CSF present on the surface of the neocortex, and a route for CSF to enter the neocortex in a healthy rat brain exists (Figure 4c).

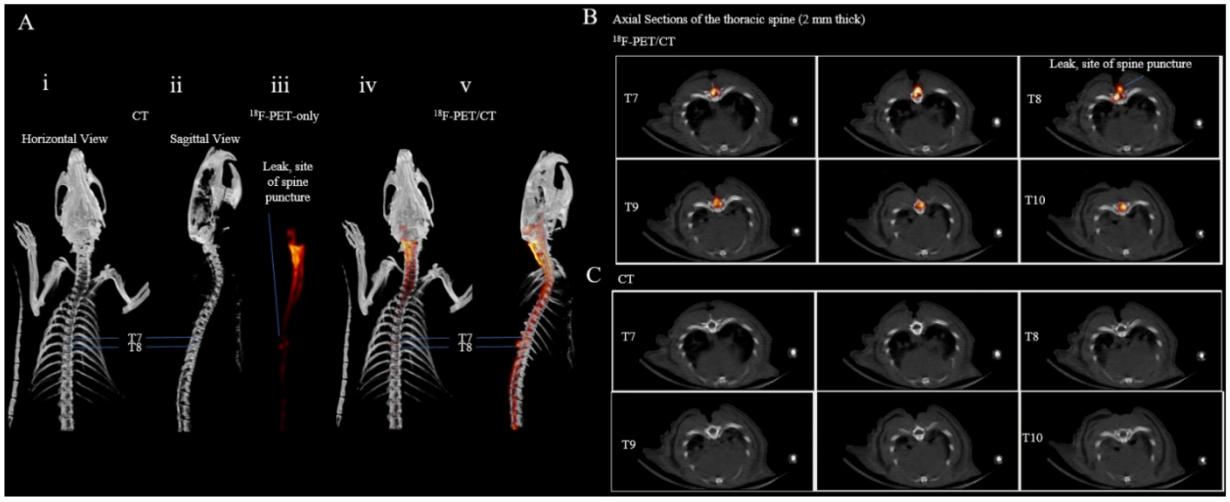

Figure 3. In a second trauma model, the thoracic spine between T7 and T8 is punctured with a 25G needle. [$^{18/19}$F]-**2** is intrathecally injected, post-trauma, and used to identify the site of spinal cord puncture that is not visible by (i) horizontal and (ii) sagittal CT. PET/CT imaging of intrathecal [$^{18/19}$F]-**2** show the leak site between T7 and T8 in (iii) maximum intensity projection PET (red), (iv) horizontal PET/CT, and (v) sagittal PET/CT. (B) Superior to inferior, axial 2.5 mm PET/CT sections of intrathecal [$^{18/19}$F]-**2** in the thoracic spine show a clear leak between T7 and T8. (C) The PET overlay is removed. Spinal defects that would indicate the site of puncture are not observable in CT. The puncture site is not obvious in CT. 4 rats were used in this study. (Additional replicates in supporting information S15, S16)

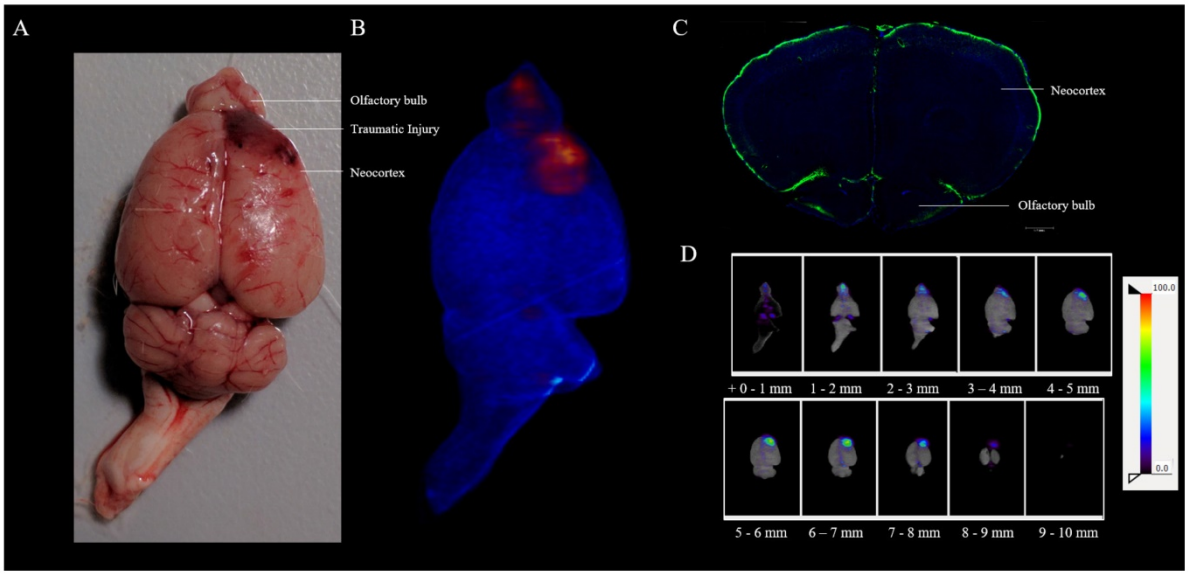

Figure 4. In a third model, [$^{18/19}$F]-**2** can be used to image traumatic brain injury. In a cryolesion-induced traumatic brain injury, the vessel walls and mater that separate the CSF from the brain are disrupted, allowing [$^{18/19}$F]-**2** and blood cells to homogenize in the brain at the site of lesion. (A) *Ex vivo* bright field image showing superficial hemorrhage on the right neocortex/olfactory bulb. This is corroborated by (B) PET (red)/CT (blue) imaging of [$^{18/19}$F]-**2** that is injected intrathecally, 10 min post-cryolesion. (C) *Ex vivo* fluorescent histology of the neocortex and olfactory bulb of a healthy (non-cryolesioned) rat that has been injected with [$^{18/19}$F]-**2.** DAPI (blue) and [^{19}F]-**2** fluorescence (green) show [^{19}F]-**2** in the CSF surrounding the brain, highlighting a route for [$^{18/19}$F]-**2** to accumulate in the neocortex following traumatic injury. (D) Horizontal 1 mm PET (NIH color table) /CT(grey) sections of (B) the brain showing signal at the site of the TBI. 1 mm sections run inferior (+0 mm) to superior (+10 mm). 3 rats were used with this trauma model, that we validate in a study with 60 mice (Additional replicate in supporting information S17) [30]

Ex vivo confirmation of CSF distribution and clearance

To confirm that [^{18}F]-**2** distributes per the CSF and colors the CSF volume both fluorescent and radioactive, rats were injected with 20-110 µCi of [^{18}F]-**2** through an intrathecal cannula. A U-100 insulin syringe was used to collect a 50 µL volume of clear, straw-colored CSF from the cisterna magna (Supporting Figure S9, 40 min post infusion)[32, 33]. The CSF containing syringe was imaged using both a Bruker extreme fluorescence camera (Figure 5a) and a LED black-light. In both cases, the collected CSF is fluorescent (PBS and FBS volumes are shown as non-fluorescent controls). To quantitate [^{18}F]-**2** in the collected CSF, the CSF containing syringe was transferred to a Wallac Wizard scintillation counter along with standards of the injectate. Based on gamma scintillation, and assuming homogeneous distribution of [^{18}F]-**2** through the CSF, we calculate that the collective CSF volume in a 200 g rat's brain and spine is 670 ± 130 µL. This value is reported with the caveat that it is likely an over estimate of the CSF volume, as [^{18}F]-**2** that is cleared from the CSF (Figure 6) would remove activity from the CSF.

To verify the presence of [^{18}F]-**2** in CSF containing volumes of the brain, rats were sacrificed 1 to 2 hours post-intrathecal injection. Brain tissues (cerebrum, brainstem, and cerebellum) were excised and placed on a petri dish along with other organs, and images were taken of the brain using a Bruker extreme (Supporting Figure S10, S11). The magna cisterna, third and fourth ventricles clearly show fluorescent signal, demonstrating that [$^{18/19}$F]-**2** distributes to the CSF volume of the brain in an intrathecal injection (Figure 5b).

To confirm that [^{19}F]-**2** is in the CSF space and is not incorporated into the cells lining the ventricles, brains containing [^{19}F]-**2** were placed in 4% paraformaldehyde/PBS at 4 °C and then sectioned into 60 µm slices with a cryotome. The slices were stained with a DAPI nuclear stain and then imaged by epifluorescent microscopy. Fluorescence originating from [^{19}F]-**2** is clearly visible in the CSF-containing ventricular space of the brain (Figure 5c). Fluorescent volumes match with CSF volumes identified in literature (contrast MR) [4, 34, 35]. Sections were then transferred to a confocal microscope and Z-stack imaging was used to show that [^{19}F]-**2** is not incorporated into the cells that contain the ventricular space (Figure 5e, Supporting Video S7).

To finally confirm that [^{18}F]-**2** is eventually cleared from the CSF and is not permanently retained by the brain and spine, rats were injected intrathecally with [^{18}F]-**2**. 2 (n=2) and 4 (n=4) hours would pass before individual organs were collected for scintillated biodistribution (Figure 6a). Biodistribution data show that [^{18}F]-**2** is cleared from the brain and spine, into the stomach and intestines, showing clearance of [^{18}F]-**2** from the CNS. This distribution is confirmed in delayed-time-point [^{18}F]-PET imaging showing that intrathecally introduced [^{18}F]-**2** clear through the gastrointestinal tract of rats (Figure 6a).

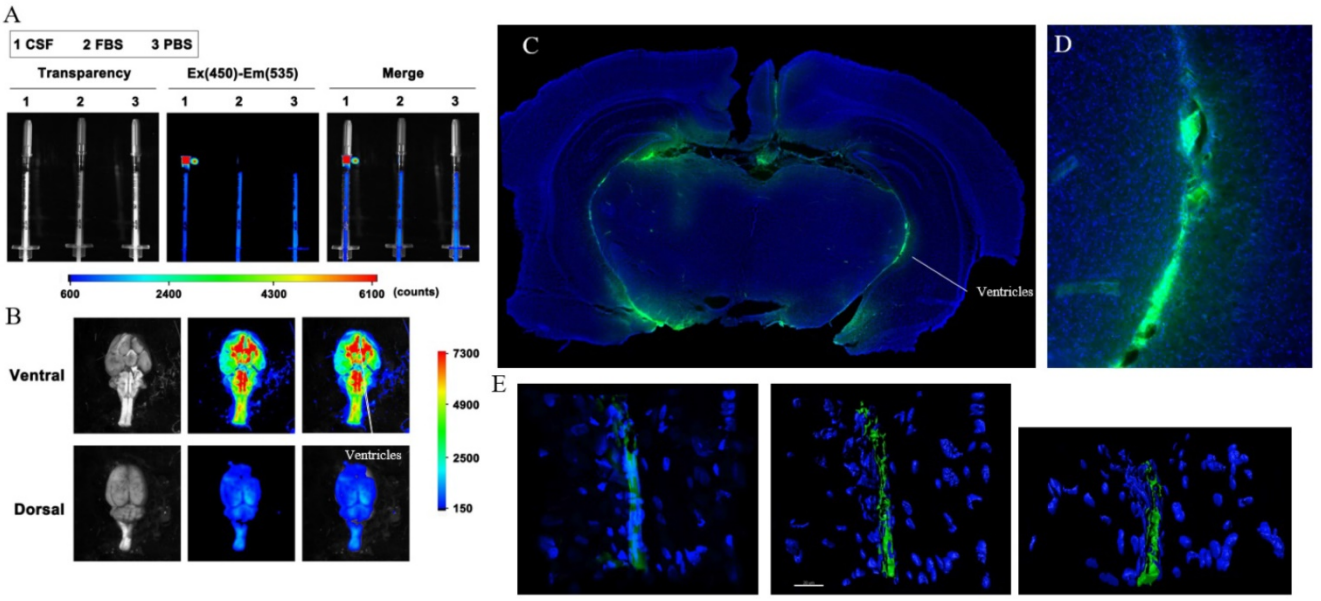

Figure 5. *Ex vivo* confirmation of [$^{18/19}$F]-**2** in the CSF. In a rat bearing intrathecal [$^{18/19}$F]-**2**, (A) CSF was drawn from the cisterna magna and analyzed for [$^{18/19}$F]-**2** fluorescence in a Bruker Extreme. CSF analyses are performed alongside FBS and PBS controls to show that signal is not due to auto fluorescence. (B) Ventral and dorsal imaging of the brain show distribution of [$^{18/19}$F]-**2** fluorescence to the ventricles and cisterns, which are caudal. (C) *Ex vivo* fluorescent histology of a coronal section (near bregma) of a healthy rat that has been injected with [$^{18/19}$F]-**2.** DAPI (blue) and [^{19}F]-**2** fluorescent signal (green) show [^{19}F]-**2** in the ventricles where CSF is present. (D) High magnification histology show [^{19}F]-**2** in the ventricle. (E) High magnification confocal microscopy is performed on the ventricle to show that [^{19}F]-**2** is present in the ventricular space, but is not taken up by the ventricle epithelium cells. 6 rats were used in this study.

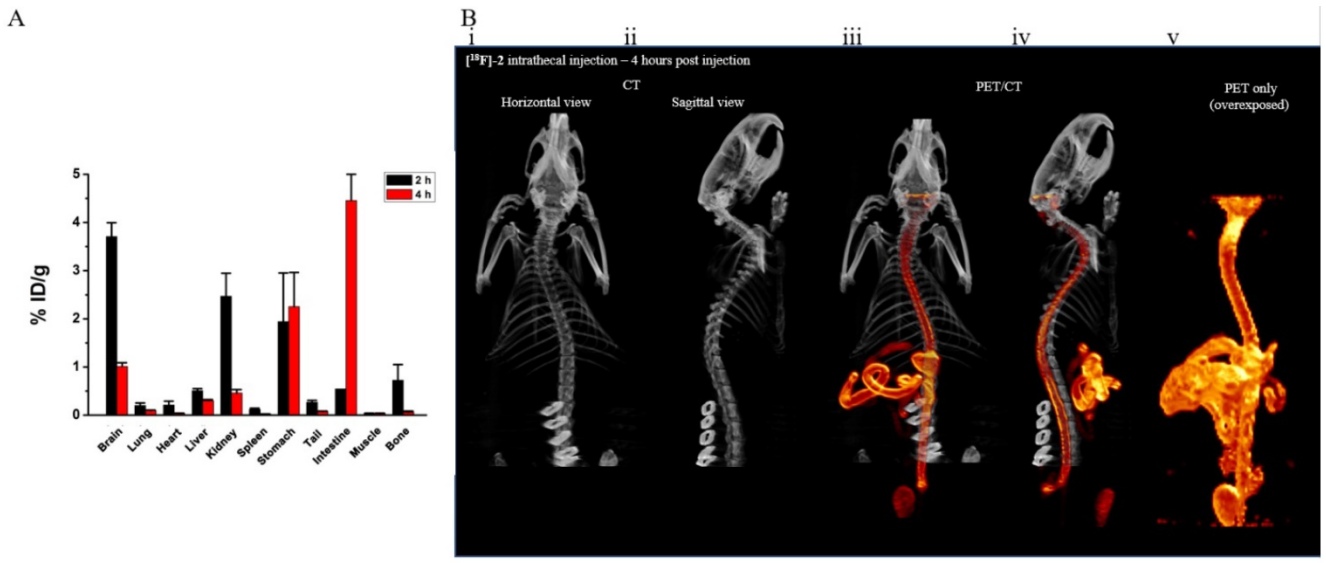

Figure 6. [$^{18/19}$F]-**2** biodistribution and confirmation of clearance. (A) biodistribution data (2h and 4h) collected in different tissues showing intrathecally injected [$^{18/19}$F]-**2** clear from the CSF and are ultimately excreted renally and through the stomach and intestines. Error – SEM. (B) (i) horizontal and (ii) sagittal CT showing the skeletal system of a rat. Late timepoint (iii) horizontal and (iv) sagittal PET/CT images (intestinal focus) of an intrathecal injection of [$^{18/19}$F]-**2** confirming clearance through the stomach and gut. (v) Deliberate PET-only overexposure of (iii) shows that [$^{18/19}$F]-**2** is stable and does not defluoridate *in vivo*. Accumulation of [$^{18/19}$F]-**2** in bone tissue (outside of the spine) is not observed. 6 rats were used in this study.

Discussion

Chemistry

The synthesis of **2** is performed in 3 steps from inexpensive, commercially available precursors. The [^{18}F]-radiolabeling of **2** is performed under acidic, isotopic exchange conditions where a non-radioactive ^{19}F atom on fluorescein is exchanged with ^{18}F-fluoride ion in water (Supporting Figure S6). Automated equipment is not necessary for radiolabeling. Facilities with access to [^{18}F]-fluoride ion (a precursor to ^{18}F-fluorodeoxy glucose and a tracer for [^{18}F]-bone scans) have the necessary equipment to perform radiolabelings. The reported chemical synthesis and radiolabeling do not require hazardous reagents and are deliberately designed to be simple, so that minimal synthetic or radiochemical skill is needed to generate [^{18}F]-**2**. Toxicity or morbidity related to [^{18}F]-**2** is not detected with [^{18}F]-**2** in over 40 rats used in the manuscript.

Considerations in probe design

The important factor in considering agents that could be used for imaging CSFL, cisternography, and myelography, is that an injection into the intrathecal space is more likely to cause morbidity and mortality than a systemically injected agent. The blood brain barrier will not prevent neurotoxicity from an intrathecally introduced agent. Additionally, injected mass is an issue. Fluorescein (>100 mg) has caused mortality in patients in the past, which is why low doses (<50 mg) are recommended in clinical IF administration [36]. This mass limit may rule out the use of new CTA and MRA contrast intrathecally. Imaging through opaque tissue like the vertebrae and skull are challenges that may limit the utility of ultrasound and photoacoustic contrast. Another major concern is a fear that [^{18}F]-**2** would not excrete or catabolize following intrathecal injection. This would lead to contrast accumulation in the brain parenchyma that could foreseeably result in delayed neurotoxicity. Because of this fear, we perform comprehensive histological (Figure 5) and survival analyses showing that [^{19}F]-**2** remains in the ventricular space and does not diffuse into the parenchyma. We perform biodistribution studies to show that [^{18}F]-**2** can be cleared from the brain (Figure 6). We also evaluate *in vitro* toxicity with immortal cell lines (Figure 1) to show that, even in the case of retention, [^{18}F]-**2** cannot cause toxicity. Others have studied ^{89}Zr and ^{124}I labeled proteins, polymers, and nanoparticles for CSF imaging by PET [37]. Nanoparticles and colloids may clear from the body more slowly than small molecules. Based on these concerns, our first choice (but not necessarily the best choice) for this project is a small-molecule, multimodality CSFL agent.

Utility in CSF leak and CSF flow detection

CSF leak can be spontaneous or caused by a wide variety of stimuli including trauma, whiplash, cervical bone spurs, hydrocephalus, and surgical intervention, including epidural procedures [38]. CSF leak is often diagnosed (and fascia repair is indicated) by intrathecally injecting an agent that can be imaged

on a SPECT scanner [39] or by observing scintillated activity (or fluorescence) that is present in nasal cavity drainage [40].

Both SPECT and fluorescent classes of agents have drawbacks. SPECT imaging requires that a patient is injected with millicurie quantities of radioactive material in the intrathecal space (cisternography). However, SPECT imaging allows the observation of a CSFL deep in a patient, through tissue that is normally opaque to fluorescence and ultrasound [41, 42]. Alternatively, fluorescence can be used to guide surgical CSF leak repair in endoscopic procedures in real time, or can inform on the qualitative status of a CSF tear, i.e. whether a tear has reopened or is adequately repaired (current paranasal CSFL surgical repair rates are 90% using fluorescent guidance). A clinician can use fluorescein in combination with an inexpensive black-light, without the need for expensive light sources, light filters (emission/excitation filters), radiochemistry, or PET/CT/MR scanning equipment. Unfortunately, the limited utility of fluorescence through deep tissue can make it difficult for a physician to pinpoint the precise intracranial location of a leak. The use of intraoperative fluorescein also has a significant false negative rate (26.2 %) [3].

Many of these drawbacks can be addressed with [$^{18/19}$F]-**2** (Figure 2). One can choose to use the non-radioactive [^{19}F]-**2** precursor in the fluorescence mode alone, where, like fluorescein, the fluorescent aspect of [^{19}F]-**2** can be used to detect and guide intranasal surgical repair. Alternatively, radioactive [^{18}F]-**2** can act as a stand-alone or co-injectate with fluorescein in radiotracer scintigraphy (pledgets) or on a PET scanner. The sensitivity of CSFL detection can be enhanced using [^{19}F]-**2** fluorescence together with [^{18}F]-**2** PET. The [^{18}F]-**2** radiolabeled product and its [^{19}F]-**2** precursor bear identical electronic structures so the two can be used in a mixture without the need to consider the complications of a compound mixture.

Comparison to other modalities

^{18}F-PET is a potentially more sensitive means of imaging CSF leak. An [^{18}F]-**2** PET/CT scan could produce higher resolution images than its ^{131}I, ^{111}In or ^{99m}Tc SPECT contrast counterparts[43]. In MR cisternography, asymmetric fluid accumulation in the right or left nostril can indicate CSFL. However, it is difficult to distinguish CSF from sinusitis [44], and there are false positives associated with MR cisternography [45]. Since the surgical approach to repairing a CSFL can be quite invasive [46], a surgeon would not use an MR image, by itself, in classifying a CSFL [47]. In MR (non-contrast) myelography [48], a volume for CSF to pool outside the spine may not exist, so low volume CSFL may not be directly imaged but instead inferred from anatomical defects. Iatrogenic trauma (introduced in a laminectomy for example) that does not produce a clear anatomical change would not be detected. MR contrast myelography is superior to non-contrast MR [49]; however, an [^{18}F]-**2** PET/CT scan does not have the same issues associated with the introduction of iodine CT or gadolinium MR contrast into the intrathecal space [50-52]. [$^{18/19}$F]-**2** is superior to the beta-2 transferrin test [53] (or other laboratory tests) for CSF leak, because PET results are immediate, and identify the exact position of a CSF tear.

We compare medical imaging modalities with the following caveat: resolution in medical imaging is complicated. A single, superior imaging modality currently does not exist [41]. This explains the mess of expensive, but required imaging equipment in our comprehensive patient care centers, including FL, US, MR, PET, CT devices. It also explains a current trend towards the development of multimodality technology e.g. PET/FL imaging [42].

A potential flaw of [^{18}F]-**2** PET vs. ^{111}In-DTPA cisternography is ^{18}F's rapid decay (4040 min vs 108 min). This rapid decay translates into a patient receiving less ionizing radiation, but complicates the ability to rescan a patient at, 24, 48, or 72 hour time-points in a very slow CSFL. Given that ^{18}F-PET is a higher resolution technique, and surgeons already inject fluorescein on the operating table, immediately before a 1-2 h surgical procedure in CSFL repair [3, 54], [^{18}F]-**2** may account for this flaw.

Current clinical fluorescein utility in CSFL diagnosis and repair demonstrates a translational application for [$^{18/19}$F]-**2**. Because [$^{18/19}$F]-**2** tracks CSF flow accurately, [$^{18/19}$F]-**2**'s fluorescent and PET aspects should have translational utility in other CSF flow applications, such as imaging flow (and detecting blockages) in ventriculoperitoneal (VP) and lumboperitoneal shunts [5-7].

Choice of an 18F-fluoride ion control, and (lack of) utility in CSFL site identification

We chose to image [^{18}F]-fluoride ion in figure 2 D-E as a control for [^{18}F]-**2** for 2 reasons: 1) SPECT emitters cannot be imaged on PET equipment (SPECT nuclide decomposition is not closely linked to quantumly entangled photon emission, which is needed for PET). And 2) Equivalent doses (20-100 μCi) of SPECT tracer on SPECT equipment do not generate the same degree of signal as a PET emitter that is imaged on a PET scanner.

[^{18}F]-fluoride ion tracks to the bone, yet [^{18}F]-fluoride ion concentration at the site of intrathecal injection (i.e. the L5-L6 vertebrae) is not

observed with [^{18}F]-fluoride ion. We believe that the tightly regulated dura mater and pia mater prevent CSF borne [^{18}F]-fluoride ion from labeling the vertebrae of the lumbar spine at the immediate injection site. The first instance that fluoride ion can interact with bone is immediately following filtration from the CSF into the paranasal vasculature[4]. This may explain observed [^{18}F]-fluoride ion accumulation at the cribriform plate (ethmoid bone, Figures 2 D-E). Concentration at the cribriform plate is not observed with [^{18}F]-**2**. The rapid filtration of [^{18}F]-fluoride ion from the CSF into the cribriform plate may explain why [^{18}F]-fluoride ion is a poor agent for localizing a site of CSFL. Alternatively, fluoride ion is very hydrophilic, so its quick diffusion from the CSF, following CSF leakage, may contribute to its poor ability to localize the site of CSFL. It should be noted that [^{18}F]-fluoride ion, like [^{111}In]-DTPA and [^{99m}Tc]-DTPA, are non-fluorescent, and cannot be utilized in intraoperative, image guided surgery. For this reason, [^{18}F]-fluoride ion and its SPECT counterparts are not precise controls for [^{18}F]-**2**. They do not serve a multimodality purpose.

Utility in other CNS applications

CSF encompasses the entire brain and spinal cord, therefore [$^{18/19}$F]-**2**'s utility should extend to myelography and TBI imaging. To illustrate this, we test [$^{18/19}$F]-**2** PET utility in two additional injury models, where injury is clear with [$^{18/19}$F]-**2** PET imaging.

In a first model (Figure 3), we induce thoracic spinal cord damage (acute spinal cord injury) by piercing the T7 - T8 intervertebrae space with a 25 G needle (Figure 3). The resulting puncture damage cannot be inferred from CT alone (deformation of the spine or misalignment of the vertebrae is not observed). However, in [$^{18/19}$F]-**2** PET, the site of puncture damage is obvious and appears as a clear deformation in maximum intensity PET/CT projections where [$^{18/19}$F]-**2** has been infused intrathecally. In a second TBI model (Figure 4), we contact the exposed skull over the right frontal neocortex with a liquid nitrogen cooled, aluminum tipped probe adapted from literature [29]. The resulting traumatic brain injury disrupts the dura mater containing CSF and the blood-brain barrier so that localized edema/hemorrhage is clearly visible in *ex vivo*, white light photography. A [$^{18/19}$F]-**2** PET scan of this brain corroborates the *ex vivo* bright field imaging. The site of hemorrhage/edema is intracranial, non-symmetric, and localized to right neocortex. Note that we recently published on the use of this cryolesion model with systemically injected [^{18}F]-labeled red blood cells (RBC) in identifying hemorrhage [30]. Although the animal model is similar, it is important to point out that [$^{18/19}$F]-**2** is very different from an [^{18}F]-labeled RBC. Here, [$^{18/19}$F]-**2** is used to image the breakdown of the meninges that contains the CSF, while the [$^{18/19}$F]-RBC is used to image breakdown of the blood vessels in the brain [30]. [$^{18/19}$F]-**2** will not distinguish between edema and hemorrhage, unlike a labeled RBC, as [$^{18/19}$F]-**2** is a small molecule that can traverse small vessel lesions that white and red blood cells cannot. Additionally, CSF flow is distributed by gravity and diffusion, so patient position is a factor in CSF TBI imaging. [$^{18/19}$F]-**2** is more likely to translate in CSFL and myelography applications vs. TBI imaging, because of positional dependence in TBI-[$^{18/19}$F]-**2** CSF imaging.

These applications show that [$^{18/19}$F]-**2** can potentially serve as a first-line imaging agent (like the CT) in identifying general CNS damage in patients**.** We show that [$^{18/19}$F]-**2** can be a more sensitive agent for detecting CNS damage than CT (myelography), and unlike other contrast imaging techniques, there are no reported life-threatening contraindications (e.g., nephrogenic systemic fibrosis) associated with the imaging of sub-microgram quantities of an ^{18}F-PET agent. This makes [$^{18/19}$F]-**2** PET immediately useful in unconscious patients, patients with incomplete or unknown histories, and in emergency department settings.

Conclusions

We report the synthesis and radiolabeling of a [$^{18/19}$F]-fluoride bearing fluorescein, **2**. Like the parent compound, fluorescein, **2** should have pre-, intra-, and post- operative utility in diagnosing CSF leak in the paranasal sinuses and otologic structures (cisternography). The PET properties of [^{18}F]-**2** make it a higher resolution, less invasive, quantitative agent that can be used to dynamically visualize CNS damage. This gives [^{18}F]-**2** additional utility in diagnosing other forms of CNS injury, where CSFL can be difficult to visualize using other imaging modalities, including acute spinal cord injury (myelography). Because of molecular similarity, and the fact that fluorescein is already of interest in many other applications in medicine, **2**-PET could be useful to other relevant fluorescein applications that are currently under investigation [15, 41, 42, 55].

Experimental Section

Synthesis

Fluorescein (F2456) and Fluorescein isothiocyanate isomer I (F4274) were purchased from Aldrich. Sterile, endotoxin and mycoplasma free,

isotonic, 1x PBS was purchased from (pH 7.4 ± 0.1, Corning Cellgro 21-040-CM).

1-(4-azidobutyl)-3-(6'-hydroxy-3,3'-dioxo-3',9a'-dihydro-3*H*-spiro[isobenzofuran-1,9'-xanthen]-6-yl)thiourea (1): To a solution of Fluorescein isothiocyanate isomer I (250 mg, 0.64 mmol) in 5 mL of dry DMF, in an oven dried 10 mL round bottom flask, 1-azido butylamine (146 mg, 1.28) was added, the reaction mixture stirred at room temperature for 12 hours or until complete consumption of starting material, as observed by UPLC-MS. The reaction mixture was transferred to a 55 mL polypropylene conical tube and 50mL of tert-Butyl methyl ether (TBME) was added to precipitate the desired product, **1**. The precipitate was filtered, and washed two more times with 10 mL of TBME. The obtained product **1**, is used in the next step without further purification. Yield (280 mg, 86%) Yellow solid. ^{1}H NMR (500 MHz, DMSO-d_6): 10.15-9.80 (m, 2H), 8.21-8.12 (m, 1H), 7.72 (d, 1H, *J* = 6.5 Hz), 7.18 (d, 1H, *J* = 8.0 Hz), 6.67 (d, 2H, *J* = 2.0 Hz), 6.61-6.55 (m, 4H), 3.54 (bs, 2H), 3.39 (t, 2H, *J* = 6.5 Hz), 1.65-1.59 (m, 4H); ^{13}C NMR (125 MHz, DMSO-d_6): 180.4, 168.5, 159.4, 158.7, 158.2, 151.8, 147.0, 141.3, 129.0, 126.5, 124.0, 116.6, 114.2, 112.5, 109.7, 102.2, 50.4, 43.5, 25.8, 25.6; HRMS (ESI): m/z calculated for $C_{25}H_{21}N_5O_5S$ + H [M + H]$^+$: 504.1336, found: 504.1336.

Trifluoro((((1-(4-(3-(6'-hydroxy-3,3'-dioxo-3',9a'-dihydro-3*H*-spiro[isobenzofuran-1,9'-xanthen]-6-yl)thioureido)butyl)-1*H*-1,2,3-triazol-4-yl)methyl)dimethylammonio)methyl)-borate (2): To a solution of 1.0 M copper sulphate (300 µL), a 1.0 M sodium ascorbate (600 µL) solution, and a solution of N, N-Di methyl N-propargyl methyltrifluoroborate (74 mg, 0.44 mmol, synthesized in one-step according to Perrin)[17] in DMF (2 mL) were added, to give a clear solution. The azide 1 (150 mg 0.30 mmol) in 1.5 mL of DMF was added last, and the reaction was stirred at 50 °C for 5 hours. Complete consumption of starting material, 1 was observed by UPLC-MS. A 1 mL volume of DMF was added to the reaction, which was filtered and purified by reverse phase HPLC using an a10-90% water-acetonitrile, 0.05% TFA, mobile phase and a Luna 10 µm C18 column (Phenomenex 00G 4253-POAX). 2 is best stored as lyophilized aliquots at -20 °C, or -78 °C, in dry conditions (Yield 280 mg, 40%) Yellow solid. ^{1}H NMR (500 MHz, DMSO-d_6): δ 10.32 (bs, 1H), 8.46-8.20 (m, 2H), 7.69 (d, 1H, *J* = 6.5 Hz), 7.10 (d, 1H, *J* = 8.0 Hz), 6.62 (d, 2H, *J* = 9.0 Hz), 6.55-6.46 (m, 3H), 4.52-4.45 (m, 4H), 3.35 (m, 2H), 2.92 (s, 6H), 2.25 (m, 2H), 1.90 (t, 2H, *J* = 9.0 Hz), 1.53 (t, 2H, *J* = 9.0 Hz); ^{13}C NMR (125 MHz, DMSO-d_6): δ 180.5, 168.5, 159.6, 159.4, 157.7, 151.8, 147.3, 141.3, 136.5, 129.0, 126.5, 124.2, 116.7, 115.4, 112.5, 109.6, 102.2, 50.5, 49.3, 43.0, 41.7, 27.2, 25.4; HRMS (ESI): m/z calculated for $C_{31}H_{32}NBF_3N_6O_5S$ + H^+ [M + H]$^+$: 669.2278, found: 669.2281.

Radiochemistry

In a typical labeling (Supporting Figure S6), a 700 µL volume of [^{18}F]-fluoride-ion-containing water (500 µL) produced from 19.2 MeV bombardment of [^{18}O]-water was flushed from a cyclotron target into a Teflon septa-sealed 5.0mL glass v-vial (Thermo Scientific Reacti-Vial #13223). The vial is transferred to a 100 °C heat block and is flushed with 40 psi N_2 gas through a 18 G inlet and passed through a 16 G tubing that is bubbled through a 1 M solution of NaOH to prevent radioactive volatilization. In 15 to 22 min, the solution of [^{18}F]-fluoride is concentrated to a <50 µL volume. It is important not to dry the [^{18}F]-fluoride completely to obtain maximum [^{18}F]-fluoride recovery.

Low activity labeling

The radiosynthesis (TOS = 0 min) was initiated with the addition of ~ 5 to 15 µL of concentrated, but not fully evaporated [^{18}F]-fluoride-ion-containing--water, with ~25 mCi of activity, to a 600 µL poly propylene PCR tube containing 80 µg (119 nmol) of [^{19}F]-**2** in 10 µl of DMSO, and 10 µL of aqueous pyridazine HCl (1.25 M, pH 2.5). This tube was heated at 50°C for 30 min. Full solubility was observed upon heating. The reaction was cooled to room temperature (end of synthesis, TOS = 30 min).

The reaction was quenched with 5% NH_4OH-Ethanol (500 µl), loaded on to 100mg of dry silica (Silicycle Silia Flash P60 (230-400 mesh)) in a cotton stoppered 1mL syringe and eluted with 5% NH_4OH -Ethanol (600 µl). 4.5 mCi of activity [^{18}F]-**2** was eluted. 4.5 mCi of activity remains trapped on the column, while 4.5 mCi of [^{18}F]-**2** is eluted (50 %). The fraction of [^{18}F]-**2** eluted contains 4.5 mCi of activity eluted with 1.5 mL of eluent. Total time for chemistry is 30 min, followed by radiochemistry (30 min) for a total of one hour.

Reverse phase HPLC on a Waters SunfireTM C18 3.5µm 4.6 x 50mm column (186002551), with a 10 min, a10-90% H_2O:ACN (0.05% TFA) gradient and a flow rate of 1 mL/min was used to confirm [^{18}F]-**2** radiolabeling and purity. Reverse phase HPLC analysis of [^{18}F]-**2** shows a single peak.

High activity labeling

A 35 µL volume of concentrated [^{18}F]-fluoride ion containing water containing 116 mCi of activity was added to a 600 µL poly propylene PCR tube containing 60 µg (75 nmol) of [^{19}F]-**2** in 20 µl of DMSO, and 10 µL of aqueous pyridazine HCl (1.25 M, pH 2.5). This tube was heated at 100°C for 30 min. The reaction was quenched with 5% NH_4OH-Ethanol (500

µl), loaded on to 100mg of dry silica in a cotton stoppered 1mL syringe and eluted with 5% NH_4OH -Ethanol (600 µl). 56.6 mCi of activity is trapped on the column, while 31.3 mCi flows through suggesting a RCY of 57%. Total time for chemistry is 30 min, followed by radiochemistry (30 min) for a total of one hour.

Recovered activity was diluted significantly with 1x PBS to give a 100 µCi of activity per 250 µL intrathecal injection. Materials were filtered through a 0.22 um syringe filter prior to injection (i.e. a 31.3 mCi, 1.5 mL dose would be diluted 1878 times with 1x PBS).

Sample size/replicates

To show that [^{19}F]-**2** is not toxic, is restricted to the CSF space in the brain and spine (in non-trauma bearing rats), and does not accumulate in the brain parenchyma, n=22 rats were used. (n=12 of 22) rats were used in survival studies, where [^{19}F]-**2** is introduced intrathecally, at 2 mM in PBS (saturating). Rats were monitored for 30 days post injection. n=2 rats were used as controls (intrathecal PBS). Morbidity and weight gain were monitored daily in survival experiments. In biodistribution studies, (n=6 of 22) rats were used to show that [$^{18/19}$F]-**2** clears from the CSF. PET/CT scanning and scintillated tissue biodistribution were used to show that [$^{18/19}$F]-**2** is cleared from the brain and spine. [$^{18/19}$F]-**2** clears through the stomach and intestine of rats. In fluorescence histology studies, (n=4 of 22) rats were used to show that [^{19}F]-**2** delivers to the CSF of the brain, and that [^{19}F]-**2** does not cross into the brain parenchyma. In experiments used to track aberrant CSF flow three different experiments were performed using n=14 rats. To produce and track aberrant CSF flow n=7 (of 14) rats were used in iatrogenic anterior skull base CSF leak experiments where, n=5 (of 14) rats were injected with [$^{18/19}$F]-**2**, and n=2 rats were injected with [^{18}F]-fluoride ion in control experiments. In the second trauma model, n=4 (of 14) rats were used to investigate puncture damage to the thoracic spine. A specific control for this model was not performed as intrathecal pre-trauma images in figure 2A (iatrogenic anterior skull base CSF leak experiments) serve as a control for thoracic spine puncture experiments (Figure 2A rat bears intrathecal [$^{18/19}$F]-**2**, but no spinal damage). Rats n=3 (of 14) were used to investigate traumatic brain injury using a cryolesion damage model. Rats n=2 were used for 99mTc-DTPA intrathecal SPECT/CT experiments. The control for this model is the cranial hemisphere that does not bear trauma. It was observed that no two-iatrogenic anterior skull base CSF leaks, thoracic puncture injuries, or TBI are identical, i.e. every model produced a different [^{18}F]-**2** PET volume.

Intrathecal catheter placement

All procedures conducted in rats were approved by the Weill Cornell Medical Center Institutional Animal Care and Use Committee (#2014-0030) and are consistent with the recommendations of the American Veterinary Medical Association and the National Institutes of Health Guide for the Care and Use of Laboratory Animals.

Sprague-Dawley rats (220-300 g) were purchased from Charles River Laboratories and acclimatized to laboratory housing condition for at least 3 days prior to experiment. Animals were anesthetized with an intraperitoneal cocktail injection of Ketamine (900 mg/kg)/Xylazine (4 mg/kg) and then placed in a prone position. The fur of the anesthetized rat around the intended incision area was shaved. A cutaneous, mid vertical incision was made in the back of the rat. The lumbar fascia and muscle on either side of L5-L6 were separated. Once the muscles are detached from L5 and L6, the dorsal aspect of L6 was removed using rongeurs to fully expose the ligament flava between L5 and L6. A needle is inserted slowly into the intraspinal space through the ligament flava. Needle insertion is halted when a tail flick is observed. The tail flick indicates correct intrathecal needle placement. A 2-3 cm length of PE-10 tubing (Instech Laboratories, Inc.) is implanted through broken ligamenta flava and should reach the lumbar enlargement of the spinal cord. The other end of catheter is threaded subcutaneously to the dorsal neck, where a rat, once woken, cannot dislodge the cannula. The cannula is exposed and fixed with a single suture in the neck. Muscle and fascia incisions are closed using sutures (4-0 silk, Henry Schein Animal Health) and the skin incision is closed with wound clips (Precise Vista 3M). Rats fully recover from this procedure in 5-7 days. Post-anesthesia mortality is not observed. Post-surgical morbidity is not observed after 7 days. Analgesics are given to rats before, during, and for 3 days, post-surgery.

Toxicity evaluation of intrathecal injection of [^{19}F]-2

After implanting an intrathecal cannula, 12 rats were randomly divided into 5 groups. Control group (n = 2) was intrathecally injected with PBS. The other 3 groups were intrathecally injected with 300 µL (n = 3), 450 µL (n = 4), 510 µL (n = 2), or 600 µL (n = 1) of saturated [^{19}F]-**2** (2 mM) at flow rate of 10 µL/min. Rats receive subcutaneous meloxicam (1 mg/kg) once a day and buprenorphine (0.05 mg/kg) twice a day after the surgery for 3 days post-operatively. The rats were weighed and observed daily, with the intent to

euthanizing rats that show any sign of paralysis or severe infection. Paralysis or infection was not observed. After 30 days of observation, rats were sacrificed with CO_2 overdose followed by bilateral thoracotomy.

[^{18}F]-2 Animal imaging

After implanting an intrathecal cannula, rats were transferred into an Inveon PET/CT and imaged by CT (10 min) followed by PET (generally 40 min). The intrathecal cannula is exposed during PET imaging, and depending on the experiment, rats could be injected with [^{18}F]-**2** during PET imaging or before placement on the Inveon PET/CT. PET/CT were processed with Amide v1.0.4 and Inveon Research Workplace. Brains were placed in 4% in paraformaldehyde solution for sectioning and macroscopic/microscopic fluorescent analyses.

Histological analysis

Rats (n=4) were injected with 250 µL of [^{19}F]-**2** (2 mM) through an intrathecal cannula. Their brains were taken out and placed in 4% in paraformaldehyde /PBS overnight at 4 °C. They were transferred into 30% sucrose solution for infiltration for 2-4 hours. A cryostat (H/I bright OTF5000) was used to generate 60-µm coronal sections that were mounted to slides with DAPI solution. The fluorescent-stained slices were scanned using Mirax 3D Histech instrument and the images were analyzed by Pannoramic Viewer 1.15.4 software.

Biodistribution

Rats (n=6) were injected with 250 µL of [^{18}F]-**2** (100 µCi) through an intrathecal cannula. At 2 or 4 hours, post injection, the rats were sacrificed by CO_2 overdose followed by bilateral thoracotomy. The main tissues were collected for scintillation measurements on a Wallac Wizard 3.0 gamma counter.

Cytotoxicity of [^{19}F]-2

A human glioblastoma cell line (U87), a human cervical cancer cell line (HeLa), a human breast cancer cell line (MDA-MB-231), and a human lung cancer cell line (A549) were cultured in DMEM (Corning) supplemented with 10% FBS (Atlanta Biological) and 100 U/mL penicillin/streptomycin (Fisher Sci.) in 5% CO_2 at 37°C. Cell proliferation was determined using a CellTiter 96® AQueous One Solution Cell Proliferation Assay (MTS, G3582, Promega). Cell lines were seeded in 96-well plates at a density of 5000 per well and incubated overnight for adhesion. Fluorescein or [^{19}F]-**2** was added into the plates at concentrations ranging from 1 nM to 100 µM. After incubation for 24 h at 37°C, the cells were rinsed with PBS and incubated for an additional 1.5 h with 100 µL of fresh medium and 10 µL MTS reagent. A 100 µL volume of supernatant was analyzed on a microplate reader (Tecan Infinite M1000 Pro). Absorbance readings were acquired at 490 nm and 630 nm. Control group viability was set to 100%.

Abbreviations

CNS: Central Nervous System; CSF: Cerebral Spinal Fluid; CSFL: Cerebral Spinal Fluid Leak; CT: Computed Tomography (no contrast); CTA: Computed Tomography Angiography (contrast); DMF: Dimethyl formamide; Fc: Fluorescein; FBS: Fetal Bovine Serum; FL: Fluorescence; IF: Intrathecal Fluorescein; MR or MRI: Magnetic Resonance Imaging (no contrast); MRA: Magnetic Resonance Angiography (contrast); NMR: Nuclear Magnetic Resonance spectroscopy; PBS: Phosphate Buffered Saline; PET: Positron Emission Tomography; SPECT: Single Photon Emission Computed Tomography; TBI: Traumatic Brain Injury; TLC: Thin Layer Chromatography; TOS: Time Of Synthesis; US: Ultrasound; UPLC-MS: Ultrahigh Pressure Liquid Chromatography- Mass Spectrometry; VP: ventriculoperitoneal

Acknowledgment

We thank Prof. Barney Yoo of the Hunter College – City university of New York, Department of Chemistry Mass Spectrometry core for high-resolution mass spectrometry data.

Funding Sources

R.T., K.H., and H.G. are funded by a National Institute of Biomedical Imaging and Bioengineering K99/R00 (EB013904). O.A. is funded in part through a NIH/NCI Cancer Center Support Grant P30 CA008748. NMR spectra were acquired with help of the WCMC NMR Core that is funded by a NIH shared instrumentation grant S10OD016320.

Author Contributions

The manuscript was written through contributions of all authors. All authors have given approval to the final version of the manuscript. H. K. performed syntheses and characterizations. H. G. performed in vitro and in vivo work including surgeries and survival studies. H. K. and H. G. performed imaging studies. B.H. and D.K. assisted in PET and SPECT image acquisition and processing. N. C., H. G., and H. K. performed in vitro viability work.

Supplementary Material

Additional File 1:
Supplementary figures.
http://www.thno.org/v07p2377s1.pdf

Additional File 2:
Video S1. http://www.thno.org/v07p2377s2.m4v
Additional File 3:
Video S2. http://www.thno.org/v07p2377s3.m4v
Additional File 4:
Video S3. http://www.thno.org/v07p2377s4.m4v
Additional File 5:
Video S4. http://www.thno.org/v07p2377s5.m4v
Additional File 6:
Video S5. http://www.thno.org/v07p2377s6.m4v
Additional File 7:
Video S6. http://www.thno.org/v07p2377s7.m4v
Additional File 8:
Video S7. http://www.thno.org/v07p2377s8.m4v
Additional File 9:
Video S8. http://www.thno.org/v07p2377s9.mp4

Competing Interests

The authors have declared that no competing interest exists.

References

1. Song Y, Li S, Song B, Zhang Y, Gao W, Li N, et al. The pathological changes in the spinal cord after dural tear with and without autologous fascia repair. Eur Spine J. 2014; 23: 1531-40.
2. Schievink WI. Misdiagnosis of spontaneous intracranial hypotension. Arch Neurol. 2003; 60: 1713-8.
3. Seth R, Rajasekaran K, Benninger MS, Batra PS. The utility of intrathecal fluorescein in cerebrospinal fluid leak repair. Otolaryngol Head Neck Surg. 2010; 143: 626-32.
4. Iliff JJ, Lee H, Yu M, Feng T, Logan J, Nedergaard M, et al. Brain-wide pathway for waste clearance captured by contrast-enhanced MRI. J Clin Invest. 2013; 123: 1299-309.
5. Sainte-Rose C, Piatt JH, Renier D, Pierre-Kahn A, Hirsch JF, Hoffman HJ, et al. Mechanical Complications in Shunts. Pediatr Neurosurg. 1991; 17: 2-9.
6. Scott M, Wycis HT, Murtagh F, Reyes V. Observations on ventricular and lumbar subarachnoid peritoneal shunts in hydrocephalus in infants. J Neurosurg. 1955; 12: 165-75.
7. Grosfeld JL, Cooney DR, Smith J, Campbell RL. Intra-Abdominal Complications Following Ventriculoperitoneal Shunt Procedures. Pediatrics. 1974; 54: 791-6.
8. Javadi SA, Samimi H, Naderi F, Shirani M. The use of low- dose intrathecal fluorescein in endoscopic repair of cerebrospinal fluid rhinorrhea. Arch Iran Med. 2013; 16: 264-6.
9. Placantonakis DG, Tabaee A, Anand VK, Hiltzik D, Schwartz TH. Safety of low-dose intrathecal fluorescein in endoscopic cranial base surgery. Neurosurgery. 2007; 61: 161-5; discussion 5-6.
10. Greitz D. Cerebrospinal fluid circulation and associated intracranial dynamics. A radiologic investigation using MR imaging and radionuclide cisternography. Acta Radiol Suppl. 1993; 386: 1-23.
11. Shetty PG, Shroff MM, Sahani DV, Kirtane MV. Evaluation of high-resolution CT and MR cisternography in the diagnosis of cerebrospinal fluid fistula. Am J Neuroradiol. 1998; 19: 633-9.
12. Wormald PJ, McDonogh M. 'Bath-plug' technique for the endoscopic management of cerebrospinal fluid leaks. J Laryngol Otol. 1997; 111: 1042-6.
13. Martin TJ, Loehrl TA. Endoscopic CSF leak repair. Curr Opin Otolaryngol Head Neck Surg. 2007; 15: 35-9.
14. Cousins MJ, Brazier D, Cook R. Intracranial hypotension caused by cervical cerebrospinal fluid leak: treatment with epidural blood patch. Anesth Analg. 2004; 98: 1794-7.
15. Nguyen QT, Tsien RY. Fluorescence-guided surgery with live molecular navigation--a new cutting edge. Nat Rev Cancer. 2013; 13: 653-62.
16. Marmor MF, Ravin JG. Fluorescein angiography: Insight and serendipity a half century ago. Arch Ophthalmol. 2011; 129: 943-8.
17. Liu ZB, Pourghiasian M, Radtke MA, Lau J, Pan JH, Dias GM, et al. An Organotrifluoroborate for Broadly Applicable One-Step F-18-Labeling. Angew Chem Int Ed. 2014; 53: 11876-80.
18. Ting R, Adam MJ, Ruth TJ, Perrin DM. Arylfluoroborates and alkylfluorosilicates as potential PET imaging agents: high-yielding aqueous biomolecular 18F-labeling. J Am Chem Soc. 2005; 127: 13094-5.
19. Ting R, Aguilera TA, Crisp JL, Hall DJ, Eckelman WC, Vera DR, et al. Fast 18F labeling of a near-infrared fluorophore enables positron emission tomography and optical imaging of sentinel lymph nodes. Bioconjug Chem. 2010; 21: 1811-9.
20. Ting R, Harwig C, auf dem Keller U, McCormick S, Austin P, Overall CM, et al. Toward [F-18]-labeled aryltrifluoroborate radiotracers: In vivo positron emission tomography imaging of stable aryltrifluoroborate clearance in mice. J Am Chem Soc. 2008; 130: 12045-55.
21. Liu Z, Lin K-S, Benard F, Pourghiasian M, Kiesewetter DO, Perrin DM, et al. One-step 18F labeling of biomolecules using organotrifluoroborates. Nat Protoc. 2015; 10: 1423-32.
22. Liu Z, Radtke MA, Wong MQ, Lin KS, Yapp DT, Perrin DM. Dual Mode Fluorescent (18)F-PET Tracers: Efficient Modular Synthesis of Rhodamine-[cRGD]2-[(18)F]-Organotrifluoroborate, Rapid, and High Yielding One-Step (18)F-Labeling at High Specific Activity, and Correlated in Vivo PET Imaging and ex Vivo Fluorescence. Bioconjug Chem. 2014; 25: 1951-62.
23. Rodriguez EA, Wang Y, Crisp JL, Vera DR, Tsien RY, Ting R. New Dioxaborolane Chemistry Enables [18F]-Positron-Emitting, Fluorescent [18F]-Multimodality Biomolecule Generation from the Solid Phase. Bioconjug Chem. 2016; 27 (5): 1390–1399.
24. Ting R, Lo J, Adam MJ, Ruth TJ, Perrin DM. Capturing aqueous [18F]-fluoride with an arylboronic ester for PET: Synthesis and aqueous stability of a fluorescent [18F]-labeled aryltrifluoroborate. J Fluor Chem. 2008; 129: 349-58.
25. Ting R, Harwig CW, Lo J, Li Y, Adam MJ, Ruth TJ, et al. Substituent effects on aryltrifluoroborate solvolysis in water: implications for Suzuki-Miyaura coupling and the design of stable (18)F-labeled aryltrifluoroborates for use in PET imaging. J Org Chem. 2008; 73: 4662-70.
26. Liu Z, Chao D, Li Y, Ting R, Oh J, Perrin DM. From Minutes to Years: Predicting Organotrifluoroborate Solvolysis Rates. Chem Eur J. 2015; 21: 3924-8.
27. Liu Z, Chen H, Chen K, Shao Y, Kiesewetter DO, Niu G, et al. Boramino acid as a marker for amino acid transporters. Sci Adv. 2015; 1: E1500694.
28. Klatzo I, Piraux A, Laskowski EJ. The relationship between edema, blood-brain-barrier and tissue elements in a local brain injury. J Neuropathol Exp Neurol. 1958; 17: 548-64.
29. Raslan F, Albert-Weißenberger C, Ernestus R-I, Kleinschnitz C, Sirén A-L. Focal brain trauma in the cryogenic lesion model in mice. Exp. Transl. Stroke Med. 2012; 4: 6.
30. Wang Y, An F-F, Chan M, Friedman B, Rodriguez EA, Tsien RY, et al. 18F-positron-emitting/fluorescent labeled erythrocytes allow imaging of internal hemorrhage in a murine intracranial hemorrhage model. J Cereb Blood Flow Metab. 2017; 37: 776-86.
31. Pogatzki EM, Zahn PK, Brennan TJ. Lumbar catheterization of the subarachnoid space with a 32-gauge polyurethane catheter in the rat. Eur J Pain. 2000; 4: 111-3.
32. Pegg CC, He C, Stroink AR, Kattner KA, Wang CX. Technique for collection of cerebrospinal fluid from the cisterna magna in rat. J Neurosci Methods. 2010; 187: 8-12.
33. Mahat MY, Fakrudeen Ali Ahamed N, Chandrasekaran S, Rajagopal S, Narayanan S, Surendran N. An improved method of transcutaneous cisterna magna puncture for cerebrospinal fluid sampling in rats. J Neurosci Methods. 2012; 211: 272-9.
34. Bakker R, Tiesinga P, Kötter R. The Scalable Brain Atlas: Instant Web-Based Access to Public Brain Atlases and Related Content. Neuroinformatics. 2015; 13: 353-66.
35. Valdes Hernandez P, Sumiyoshi A, Nonaka H, Haga R, Aubert Vasquez E, Ogawa T, et al. An in vivo MRI Template Set for Morphometry, Tissue Segmentation, and fMRI Localization in Rats. Front Neuroinform. 2011; 5: 26.
36. Felisati G, Bianchi A, Lozza P, Portaleone S. Italian multicentre study on intrathecal fluorescein for craniosinusal fistulae. Acta Otorhinolaryngol Ital. 2008; 28: 159-63.
37. Papisov M, Velov V, Fishchman A, Bonab A, Levine D, Shi R. The dynamics of intrathecal bolus and cerebrospinal solute transport. J Nucl Med. 2015; 56: 1555.
38. Schievink WI. Spontaneous spinal cerebrospinal fluid leaks and intracranial hypotension. JAMA. 2006; 295: 2286-96.
39. Ali SA, Cesani F, Zuckermann JA, Nusynowitz ML, Chaljub G. Spinal-cerebrospinal fluid leak demonstrated by radiopharmaceutical cisternography. Clin Nucl Med. 1998; 23: 152-5.
40. Ashburn WL, Harbert JC, Briner WH, Di Chiro G. Cerebrospinal fluid rhinorrhea studied with the gamma scintillation camera. J Nucl Med. 1968; 9: 523-9.
41. Tsien RY. Imagining imaging's future. Nat Rev Mol Cell Biol. 2003; Suppl: SS16-21.
42. An F-F, Chan M, Kommidi H, Ting R. Dual PET and Near-Infrared Fluorescence Imaging Probes as Tools for Imaging in Oncology. Am J Roentgenol. 2016; 207: 266-273.
43. Rahmim A, Zaidi H. PET versus SPECT: strengths, limitations and challenges. Nucl Med Commun. 2008; 29: 193-207.
44. Melamed J, Stone B, Beaucher WN. Spontaneous cerebrospinal fluid rhinorrhea with associated sinusitis and allergic rhinitis. Allergy Proc. 1994; 15: 197-200.
45. Tan XL, Yang QD, Liu XJ, Xiao B, Tang BS. Teaching NeuroImages: False-positive magnetic resonance sign in spontaneous spinal CSF leak. Neurology. 2011; 76: e15.
46. Vazquez A. Endoscopic CSF Leak Repair. You Tube: Google; 2015.

47. Har-El G. What is "Spontaneous" Cerebrospinal Fluid Rhinorrhea? Classification of Cerebrospinal Fluid Leaks. Ann Otol Rhinol Laryngol. 1999; 108: 323-6.
48. Nagayama M, Watanabe Y, Okumura A, Amoh Y, Nakashita S, Dodo Y. High-Resolution Single-Slice MR Myelography. Am J Roentgenol. 2002; 179: 515-21.
49. Chazen JL, Talbott JF, Lantos JE, Dillon WP. MR Myelography for Identification of Spinal CSF Leak in Spontaneous Intracranial Hypotension. Am J Neuroradiol. 2014; 35: 2007-12
50. Takahashi M, Tsutsui H, Murayama C, Miyazawa T, Fritz-Zieroth B. Neurotoxicity of gadolinium contrast agents for magnetic resonance imaging in rats with osmotically disrupted blood-brain barrier. Magn Reson Imaging. 1996; 14: 619-23.
51. Feng X, Xia Q, Yuan L, Yang X, Wang K. Impaired mitochondrial function and oxidative stress in rat cortical neurons: implications for gadolinium-induced neurotoxicity. Neurotoxicology. 2010; 31: 391-8.
52. Junck L, Marshall WH. Neurotoxicity of radiological contrast agents. Ann Neurol. 1983; 13: 469-84.
53. Skedros DG, Cass SP, Hirsch BE, Kelly RH. Beta-2 transferrin assay in clinical management of cerebral spinal fluid and perilymphatic fluid leaks. J Otolaryngol. 1993; 22: 341-4.
54. Raza SM, Banu MA, Donaldson A, Patel KS, Anand VK, Schwartz TH. Sensitivity and specificity of intrathecal fluorescein and white light excitation for detecting intraoperative cerebrospinal fluid leak in endoscopic skull base surgery: a prospective study. J Neurosurg. 2016; 124: 621-6.
55. Wu AP, Whitney MA, Crisp JL, Friedman B, Tsien RY, Nguyen QT. Improved facial nerve identification with novel fluorescently labeled probe. Laryngoscope. 2011; 121: 805-10.